Contents lists available at ScienceDirect

Materials Today Bio

Shape-defined solid micro-objects from poly(D,L-lactic acid) as cell-supportive counterparts in bottom-up tissue engineering

A.M. Leferink [a,b,d], M.P. Tibbe [b,d], E.G.B.M. Bossink [b], L.E. de Heus [a,b], H. van Vossen [c], A. van den Berg [b], L. Moroni [d], R.K. Truckenmüller [d,e,*]

[a] Applied Stem Cell Technologies Group, TechMed Centre, University of Twente, 7500 AE, Enschede, the Netherlands
[b] BIOS/Lab on a Chip Group, TechMed Centre and MESA + Institute for Nanotechnology, University of Twente, 7500 AE, Enschede, the Netherlands
[c] MESA + NanoLab, MESA + Institute for Nanotechnology, University of Twente, 7500 AE, Enschede, the Netherlands
[d] Department of Complex Tissue Regeneration, MERLN Institute for Technology-Inspired Regenerative Medicine, Maastricht University, 6229 ER, Maastricht, the Netherlands
[e] Department of Instructive Biomaterials Engineering, MERLN Institute for Technology-Inspired Regenerative Medicine, Maastricht University, 6229 ER, Maastricht, the Netherlands

ARTICLE INFO

ABSTRACT

In bottom-up tissue engineering, small modular units of cells and biomaterials are assembled toward larger and more complex ones. In conjunction with a new implementation of this approach, a novel method to fabricate microscale objects from biopolymers by thermal imprinting on water-soluble sacrificial layers is presented. By this means, geometrically well-defined objects could be obtained without involving toxic agents in the form of photoinitiators. The micro-objects were used as cell-adhesive substrates and cell spacers in engineered tissues created by cell-guided assembly of the objects. Such constructs can be applied both for *in vitro* studies and clinical treatments. Clinically relevantly sized aggregates comprised of cells and micro-objects retained their viability up to 2 weeks of culture. The aggregation behavior of cells and objects showed to depend on the type and number of cells applied. To demonstrate the micro-objects' potential for engineering vascularized tissues, small aggregates of human bone marrow stromal cells (hMSCs) and micro-objects were coated with a layer of human umbilical vein endothelial cells (HUVECs) and fused into larger tissue constructs, resulting in HUVEC-rich regions at the aggregates' interfaces. This three-dimensional network-type spatial cellular organization could foster the establishment of (premature) vascular structures as a vital prerequisite of, for example, bottom-up-engineered bone-like tissue.

1. Introduction

Tissue engineering (TE) typically makes use of a combination of porous scaffolds from biomaterials of synthetic or biological origin, growth factors and the patient's own cells to ultimately repair or replace diseased, damaged, or lost tissue [1–3]. The scaffolds provide an environment for cells to adhere and proliferate, which at the same time provides mechanical stability, particularly in hard-tissue replacement, and supports the cells to ultimately gain and retain the desired function.

Engineering tissues *in vitro* can be subdivided into the classical top-down and the more recent bottom-up TE [4–6]. In top-down TE, a tissue construct is engineered with respect to, among others, size and shape of the tissue to be restored. These tissue constructs generally comprise a correspondingly large, one-piece porous biomaterial serving as a scaffold when adding cells. A disadvantage when using the top-down approach lies in the often obtained inhomogeneous cell distribution throughout the scaffold [7]. Furthermore, most top-down approaches do not allow for a high degree of tissue complexity, for example, by applying multiple cell types while controlling their spatial organization, and also not for an early dynamic tissue remodeling before the single-piece, static scaffold is degrading. Moreover, top-down TE typically requires invasive procedures to be able to implant the reconstructed tissue in the defect site *in vivo*.

In contrast, traditional bottom-up TE overcomes some of these problems by, for example, embedding cells in a hydrogel in which they can be distributed homogeneously when mixing them with the
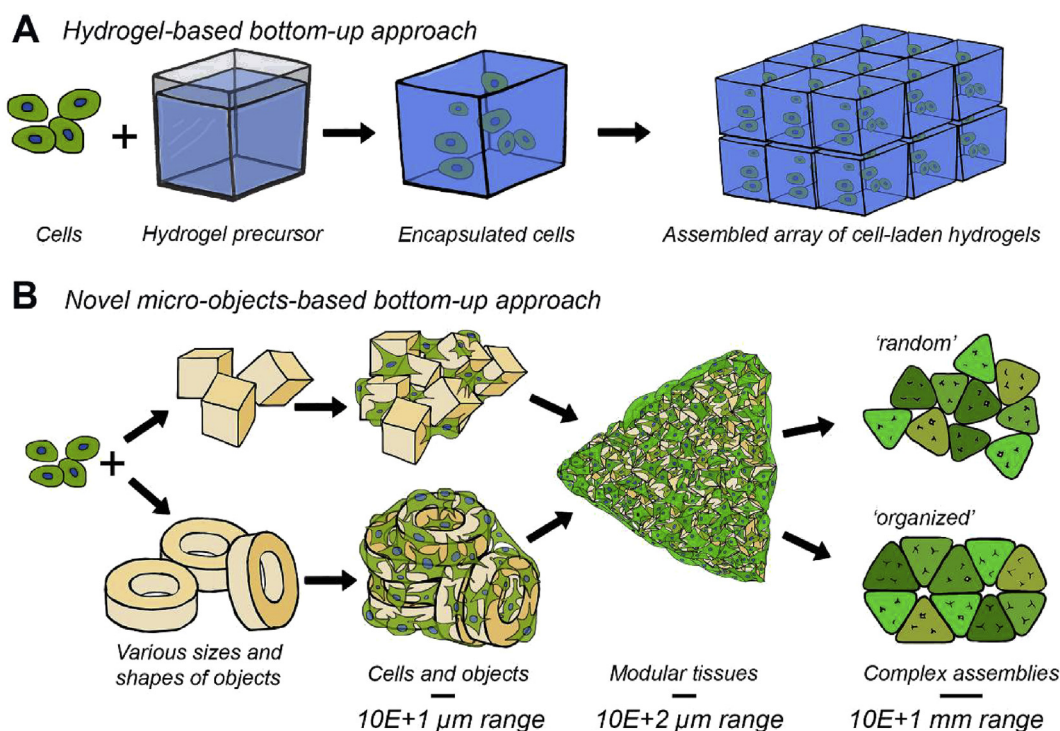

Fig. 1. Visual comparison of the (A) traditional gel-based bottom-up TE approach and the (B) novel 'solid' particles–based bottom-up TE approach presented in this article. (A) Well-known hydrogel-based bottom-up approaches provide cells with structural support and allow for high control of constructs' architecture by assembling cell-laden building blocks [11]. (B) Here, cells are combined with micro-objects of different shapes and sizes to create millimeter-sized modular tissues. In these modules, the objects are occupying space, which considerably lowers the number of required cells to obtain clinically relevantly sized tissue constructs compared with a cell-only approach (the latter is not shown in the figure). Furthermore, these objects provide surface area for cell attachment. The formed tissue modules can be obtained in various shapes and sizes depending on the mold in which they are allowed to self-assemble. By combining multiple tissue modules, larger, millimeter-sized, and more complex tissue constructs can be created. TE, tissue engineering.

corresponding precursor before gelation and which can enable much earlier remodeling (Fig. 1A) [8–12]. Griffin et al. [13] have reported a bottom-up method in which cells are not encapsulated inside hydrogels but reside in between self-assembled hydrogel-based spheres. In that study, the cells show a homogenous distribution between the spheres and remain highly accessible for nutrient and gas supply and metabolic waste exchange in a wound healing application. Yet, hydrogels have a limited mechanical stability and typically a high degradation rate, making them inapplicable for load-bearing applications, such as in bone TE, or as long-term cell support. To overcome this well-known limitation in the mechanical properties of hydrogels, already before the aforementioned study, we introduced a method to create cell-assemblable micro-objects from the relatively stiff, epoxy-based polymer SU-8 [14]. Although SU-8 has a documented biocompatibility [15,16], the fact that the objects were made by photolithography poses the risk of toxic traces [17], in the form of free radicals, which might (unnoticedly) bias readouts in applications of the micro-objects in three-dimensional (3D) *in vitro* models for research purposes and would make it difficult to get objects from this material approved for clinical applications.

Therefore, we developed a novel, radical-free method based on a combination of hot embossing [18], or thermal imprinting, and reactive ion etching (RIE), known as (nano)imprint lithography (NIL) [19,20]. The imprinting was performed on a poly(D,L-lactic acid) (PDLLA) film placed on a water-soluble sacrificial layer, to create free- or isolated standing and releasable engineered micro-objects. Medical-grade PDLLA was chosen as an exemplary or model thermoplastic biopolymer in conjunction with its comparatively low material costs, good thermal processability, and suitable, for example, mechanical properties and clinical relevance in the already mentioned field of bone TE [21,22].

In this potential main area for clinical application, the engineered micro-objects could, for example, be a component of an injectable formulation to treat or fill critical-size bone defects [14]. But also in other TE fields, for example, where conventional scaffolds in the form of porous biomaterials are researched so far, micro-objects from similar materials can, with the cells and the extracellular matrix (ECM) deposited by them acting as a binder for the objects, provide comparable material-based initial mechanical support or stability to the engineered tissues. At the same time, in contrast to the static macro-scale scaffolds, the microscale objects – as dynamic scaffolding entities that can be moved by the cells – allow immediate local remodeling of the cell-material construct and might even give it more flexible and adaptive biomechanical properties as a whole. In a previous study, the bottom-up TE of tubular structures scaffolded by micro-objects could be demonstrated [14], as they could similarly represent a potential preliminary stage of a future tissue-engineered trachea or ureter. Another application field could be the use of the objects as advanced cell expansion carriers, particularly when provided with engineered cell-instructive surfaces, for example, by micro- or nanoimprinting, as a result of a previous screen of such surfaces condensed on a miniaturized library created by means of the same imprint technology [23]. Last but not least, as already suggested, the micro-objects could be used in 3D *in vitro* research models, as similarly demonstrated in the present study. When doing so, the objects could, for example, bring the powerful instructive potential of micro- and nanoengineered surfaces [24,25] to the third dimension when after the objects' highly defined creation, including such engineered surfaces, on wafer-type 2D technical substrates releasing the objects from the substrates and aggregating them with cells in a full 3D fashion.

The PDLLA objects were fabricated in three different shapes as a mean to vary the amount of material per overall volume. The objects were used as cell-adherent substrates and cell spacers in engineered tissues created by cell-guided assembly (Fig. 1B). These constructs can then be

aggregated into (geometric) modular tissues, which in turn can be further applied as building blocks to construct larger and more complex, random or organized assemblies. In such aggregates or assemblies, the micro-objects are expected to avoid (too) high cell or tissue contraction as observed in cells-only bottom-up TE approaches [26–28]. This contraction otherwise may hamper integration with surrounding tissues after implantation.

2. Materials and methods

2.1. Microfabrication process of micro-objects

2.1.1. Dip-coating and film transfer

Fig. 2 shows a simplified representation of the required steps in the microfabrication process. Polymer films from PDLLA (Purasorb 7028; Corbion) were obtained by vertically dipping a 4-inch stainless-steel wafer into a solution of (9% w v^{-1}) dichloromethane (DCM; Sigma-Aldrich) and withdrawing it from the solution with a speed of 40 mm/min (Fig. 2A). After 30 min of solvent evaporation, the dip-coated PDLLA film was transferred from the stainless-steel wafer and laminated onto a precoated 4-inch silicon wafer (Fig. 2B). The coating consisted of a layer of Omnicoat™ (MicroChem), which was spun onto the silicon wafer with a speed of 3000 rpm for 30 s and baked at 180 °C for 1 min to let residual solvent evaporate. This Omnicoat™ layer was applied to improve the adherence of the second layer consisting of poly(vinyl alcohol) (PVA; Mw: 13,000–23,000; Sigma-Aldrich). The PVA was dissolved in dH$_2$O (5% w v^{-1}) and filtered (mesh size: 0.2 μm) before application. The PVA layer was spun on top of the Omnicoat™ layer with a speed of 2000 rpm for 30 s and baked for 15 min at 120 °C. The PVA coating acts both as a promoter for the adhesion of the PDLLA film to the wafer and as a water-soluble sacrificial layer in the object release process after patterning the film.

2.1.2. Mold fabrication and imprinting

Micromolds based on 4-inch silicon wafers and containing arrays of cavities for replicating three different shapes of micro-objects (cubes, donut-, and LEGO™-like objects) were made by standard UV lithography followed by deep RIE (AMS 100SE; Adixen). To facilitate demolding, an antisticking coating of perfluorooctyltrichlorosilane (FOTS; Sigma-Aldrich) was applied to the molds. The laminated PDLLA film was imprinted between the mold and the PVA layer with a pressure of 30 bar for 10 min at a temperature of 130 °C using a dedicated machine for hot embossing NIL (EITRE® 6; Obducat) (Fig. 2C). Demolding was

performed manually. Surface profiles of the imprinted film and the applied mold were acquired using a white light interferometer (Contour GT-I; Bruker) to confirm a complete filling of the mold.

2.1.3. Etching and release

A directional oxygen plasma etch was carried out on an in-house-built RIE machine (TEtske; TCO, MESA + Institute for Nanotechnology, University of Twente) (Fig. 2D). An electrode temperature of 10 °C, an O$_2$ flow of 50 sccm, a pressure of 10 mTorr, and a power of 50 W resulted in an etch rate of approximately 500 nm/min for 95% load. These settings were applied for 15 min to remove the thin residual layer of PDLLA that is left on the substrate wafer between the objects after imprinting. After residual layer removal, the wafer displayed free-standing objects, which could be released from the wafer by immersing it into a Teflon® Petri dish with demi water (Fig. 2E). Gently agitating the dish caused the PVA layer underneath the objects to be dissolved, leading to the release of the objects. The objects were washed multiple times in demi water and ethanol to remove PVA from their surfaces and to leach potentially remaining solvent traces still from dip-coating out of their bulk. To remove possible contaminants or (still) interconnected objects, the object suspension was washed 3 times with demi water and passed over microsieves (mesh size depending on the size of the objects), followed by washing for 5 times in 70% ethanol. Before culture, the objects were washed with phosphate-buffered saline (PBS) twice and incubated in cell type-dependent culture media for at least 18 h before adding cells. To assess the surface profile and roughness of the micro-objects after etching and release, atomic force microscopy (AFM) analysis was conducted on a donut-shaped micro-object.

2.2. Formation of cell and micro-object assemblies

2.2.1. Cell culture and media

Human bone marrow stromal cells (hMSCs) were isolated and proliferated as described previously [29]. Bone marrow aspirates were obtained from patients who had given written informed consent. Briefly, aspirates were cultured in minimal essential medium (α-mem; Gibco, Life Technologies) complemented with 10% v/v heat-inactivated fetal bovine serum (FBS; SA origin; Sigma-Aldrich), 100 U mL^{-1} of penicillin and 100 μg mL^{-1} of streptomycin (pen/strep; Gibco), 0.2 mM L-ascorbic acid 2-phosphate magnesium salt (ASAP; Sigma-Aldrich), and 1 ng mL^{-1} of basic fibroblast growth factor (bFGF; Isokine).

Human umbilical vein endothelial cells (HUVECs, ATCC) were cultured in endothelial cell growth medium (EGM-2; Gibco). While
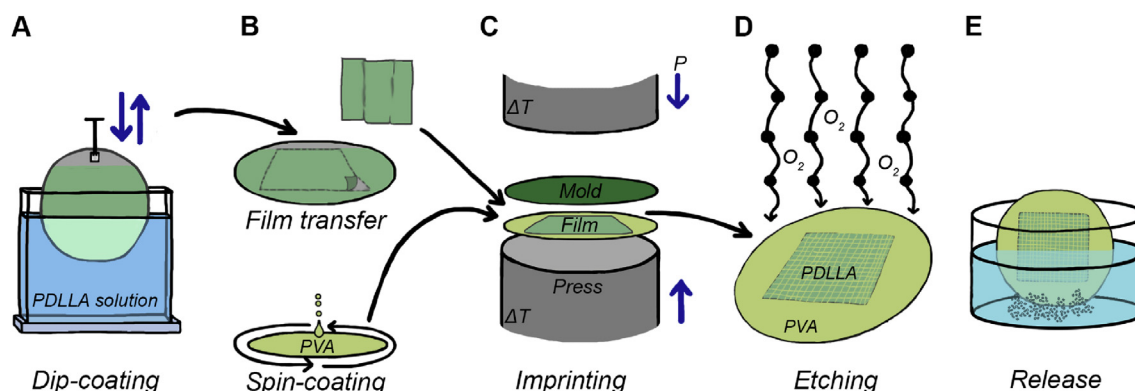

Fig. 2. A schematic representation of the five sequential processing steps to fabricate free-floating PDLLA-based micro-objects. (A) PDLLA was dissolved in DCM (9% w v^{-1}). PDLLA films with a thickness of approximately 5 μm were created from this solution on a stainless-steel wafer by dip-coating. (B) Before imprinting, the dip-coated PDLLA film was peeled of the stainless-steel wafer and transferred onto a silicon wafer, which before was spin-coated with a layer of PVA. (C) As a mold, a silicon wafer containing the inverse structures of the micro-objects to be molded and coated with an FOTS antisticking layer was applied. Micro-objects were thermally imprinted under vacuum at a temperature of 130 °C. (D) The imprinted micro-objects were then still connected through a residual layer of PDLLA, which was removed by directional oxygen plasma etching. (E) After etching, free-floating micro-objects were obtained by dissolving the sacrificial PVA layer underneath the objects when immersing the wafer in demi water. PDLLA, poly(D,L-lactic acid); DCM, dichloromethane; PVA, poly(vinyl alcohol); FOTS, perfluorooctyltrichlorosilane.

cocultured cells, a mixture of α-mem and EGM-2 medium (1:1) was used. In cases in which solely hMSCs or HUVECs were cultured, α-mem and EGM-2 medium were used, respectively.

2.2.2. Agarose-coated well plates and agarose microwell arrays

To obtain hemispherically shaped cell-repellent layers, a solution of agarose (2% w v^{-1}; UltraPure; Thermo Scientific) in PBS was added to conventional flat-bottom 96-well plates to form a gel. A similar solution was applied to obtain microwell arrays by means of casting the agarose solution on a patterned polydimethylsiloxane (PDMS) disk. This PDMS disk was prepared by curing PDMS solution in a Plexiglas® mold, which in turn was patterned by means of an in-house-built microdrilling device.

2.2.3. Live-dead staining

Cell viability was assessed by staining the aggregates with 5 μg mL^{-1} of calcein AM (Thermo Fisher Scientific) and 40 μg mL^{-1} of propidium iodide (PI; Sigma-Aldrich) stains, where calcein AM stains viable cells green and PI stains nuclei of necrotic and apoptotic cells red. The stained aggregates were imaged by fluorescence microscopy (EVOS FL; Life Technology).

2.2.4. Cell tracker

To distinguish the two cell types (hMSCs and HUVECs) in coculture, they were labeled with Vybrant Di-I (red) and Di-O (green) cell tracker dyes (Molecular Probes, Invitrogen). To label the cells, 1×10^6 cells mL^{-1} were resuspended in serum-free medium developed at Roswell Park Memorial Institute (RPMI) and 5 μL of dye solution was added per milliliter of cell suspension. While labeling, the cell suspension was incubated for 20 min at 37 °C. The cell suspension was centrifuged at 390 $\times g$ for 5 min, and the supernatant was aspired. Afterward, the cells were resuspended in RPMI and the centrifugation steps were repeated for another 2 times. After seeding the cells, a recovery time of at least 10 min was taken into account before imaging the cells.

2.2.5. Scanning electron microscopy (SEM)

Cellular attachment and distribution within the hMSC-micro-object aggregates were characterized by scanning electron microscopy (SEM) analysis (XL 30 ESEM-FEG; Philips). After 7 days of culture, the aggregates were fixed for 30 min in 10% formalin. The fixated aggregates were dehydrated in sequential ethanol series and critical point-dried from liquid carbon dioxide (CPD 030 Critical Point Dryer; Balzers). The dried aggregates were gold sputter-coated (108auto; Cressington) before SEM analysis. SEM images were obtained with an acceleration voltage of 30 kV and a working distance of 10 mm.

2.2.6. Histology

After 1 week of culture, unless stated otherwise, aggregates were fixed for 30 min in 10% formalin and stored in PBS at 5 °C until further processing. Samples were dehydrated using a sequential ethanol series (60, 70, 80, 90, 96, and 100% ethanol; 30 min for each step) and subsequently embedded in glycol methacrylate (GMA). The obtained blocks were sectioned at 5-μm intervals and stained with hematoxylin and eosin (Sigma-Aldrich) for visualization of the nuclei and cytoplasm, respectively. The stained sections were imaged using bright-field microscopy (Nanozoomer; Hamamatsu).

2.3. Image analysis

Circularity was quantified using ImageJ [30]. The projection area *A* and the corresponding perimeter *p* of the aggregates were analyzed and measured. Circularity was then calculated as a function of *A* and *p*, following Eq. (1).

$$Circularity[\%] = (4\pi A / p^2) \; x \; 100\% \qquad \text{(Equation 1)}$$

2.4. Statistical analysis

Results are presented as mean ± standard deviation and compared using one-way analysis of variance (multiple conditions) with a Bonferroni post-test. Statistical significance was set to a *p*-value < 0.05 (*).

3. Results and discussion

3.1. Microfabrication process

A large amount of approximately 2.5×10^6 objects is obtained within one imprinting cycle after which they are still connected by a thin residual layer (Fig. 2B). Along with the design of the mold, the optimal thickness of the dip-coated polymer film was calculated to minimize the thickness of the residual interconnecting layer without compromising the mold filling and consequently the replication fidelity. In this conjunction, the aforementioned uniformity of the polymer film thickness is crucial. In literature, several approaches to obtain free-standing or residual layer-free micro-objects in connection with polymer micromolding or -replication are proposed [31]. These are, among others, based on selective mold functionalization and filling followed by microtransfer molding or related printing processes [32–34], through-thickness embossing with a rubber-assisted ejection mechanism [35], or (micro)punching [36].

In the process presented here, similar to original NIL, an optimized oxygen plasma etch protocol removes the residual layer between the micro-objects after demolding the imprint (Fig. 2C), while simultaneously etching the top part of the objects. This renders the objects slightly more hydrophilic on all accessible sides because of the introduction of oxygen-containing groups and roughness on the surface. A surface profile plot of the mold and of the imprinted polymer film before oxygen plasma etching was obtained by white light interferometry (Fig. S1). The imprinted film showed the inverted surface profile of the mold, indicating a successful filling of the mold and a successful demolding of the imprinted film. By removal of the residual layer by plasma etching, free-standing PDLLA micro-objects were obtained. After etching, a surface scan was performed by AFM (Fig. S2). The height profile on the top of the object, which appears as a sort of rim, is a result of the mold fabrication process. The fact that this irregularity is conserved after oxygen plasma etching shows the high degree of directionality of the oxygen plasma etching procedure. The underlying sacrificial layer from PVA was dissolved in demi water, releasing the micro-objects from the wafer (Fig. 2D).

As indicated, PDLLA was chosen as a model thermoplastic biopolymer and can be substituted by every other biocompatible thermoplastic. PDLLA is known to form acidic products during its usually desired degradation. When about 1×10^7 cube-shaped objects, corresponding to approximately 0.32 cm^3 total volume, were stored immersed in 5 mL of deionized (DI) water at room temperature, after 6 months, no change in the pH of the DI water could be observed. Although the degradation behavior of the material has to be assumed to be different under physiological conditions *in vivo*, it is expected that waste products can be cleared at a sufficient rate to prevent tissue damage and that cells will have ample time to express their own mechanically supporting extracellular matrix scaffold. Regarding the latter, we anticipate that material degradation and taking over of the material's mechanical stabilization role by formed tissue will be more uniform for many microscaffolds than for a single macroscopic scaffold. This should be particularly the case for polymers rather undergoing bulk than surface degradation, such as the chosen PDLLA, where the sudden structural collapse of a bigger volumetric construct might be critical in comparison with the gradual resorption of many well-distributed small centers of degradation.

In case other materials are preferred for a specific biomedical application, in principle, as indicated, every other amorphous thermoplastic biopolymer can be used and processed, both biodegradable and bioinert ones. For example, the bioresorbable polymers poly-(lactic-co-glycolic

acid) (PLGA) and poly-(1,3-trimethylene carbonate) (PTMC) have already shown a good compatibility with hot embossing and NIL-based procedures [37]. For the suggested applications of the micro-objects in the fields of *in vitro* models or cell expansion, biostable materials could be preferable. The probably most trusted material in this concern, (tissue culture) polystyrene, was shown by us to be also processable by micro-imprinting [38], the process also used for PDLLA in this study (even the same equipment was used). For each polymer, the method has of course to be optimized with respect to dip-coating, film transfer, spin-coating (of a sacrificial layer material and the affinity to it to ensure proper demolding after the imprint), imprinting, and etching parameters. The decoupling of making the film to be imprinted on a first substrate and the sacrificial layer on a second one, in each case from dissolved polymers, circumvents problems, such as local thickness variations of the two materials, related to a (partial) dissolution of the sacrificial material during coating of the material to be imprinted. This opens up many possibilities concerning material choice. Crystallinity of the polymer should be avoided because it can lead to an inhomogeneous progress of the plasma etching for residual layer removal, also affecting the surface roughness of the micro-objects.

3.2. Shapes and sizes of the micro-objects

Previously, we could show that by varying the shape and size of objects and the ratio of cells to objects, the compaction of the aggregates could be altered [14]. Consequential changes of the aggregates'

permeability may in turn change the cells' survivability within the aggregates. Many other studies have revealed the influence of substrate geometry, or shape, and topography, both at a micro- and nanoscale, on the morphology of cells and thus their function [24,39,40]. To demonstrate the degree of freedom in terms of object shapes that can be realized using the fabrication method described here, besides cubes, also donut- and LEGO™-shaped micro-objects were fabricated (Figs. 3A–C). In case of the latter two shapes, open free volume is introduced in the objects that cannot be occupied by other objects upon assembly and therefore has an impact on aggregate compaction. Instead, the volume(s) can be entered by cells, or (temporarily) perfused by culture medium or interstitial fluid. The many microlumens do not only introduce a large surface-to-volume ratio that can be beneficial for cell adherence but could also aid (nutrient) diffusion. The corresponding mold designs can be found in Fig. S3. Many more shapes and sizes of micro-objects can be realized by this method with freedom of design in so-called '2.5D', namely, in 2D with the third dimension only being variable over an entire object but not within the same. The dimensionality of the 2.5D micro-objects is increased by them being dynamically (re-)arranged by the cells and thereby also being rotated (Figs. 3F–J). Micro-objects that are more three-dimensional, with surfaces stepped, sloped, or curved out of the mold(ing) plane, can be replicated in mold cavities being created, for example, by various 3D silicon micromachining technologies [41], or two-photon polymerization laser lithography [42] on a suitable substrate for the creation of a master mold in combination with copying the master into a working mold.
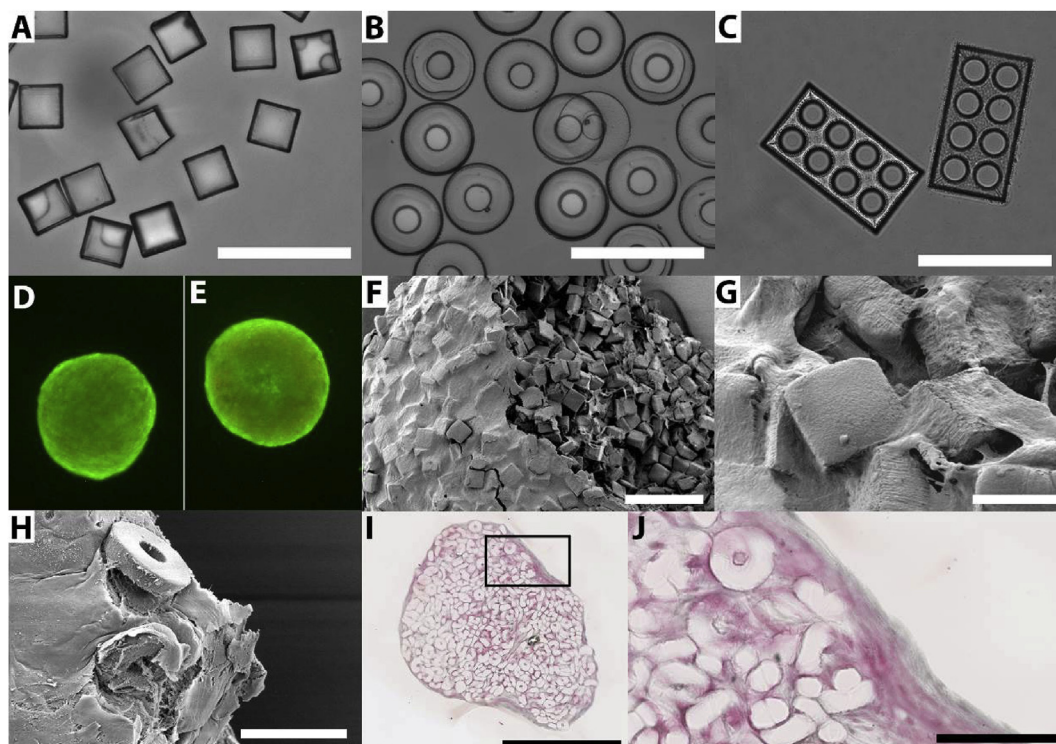

Fig. 3. Micro-objects of different defined shapes such as (A) cubes, (B) donut-, and (C) LEGO™-shaped (porous) objects can be obtained and are shown here in suspension in culture medium to incubate them before cell seeding. A live-dead assay on the full aggregate of 5×10^4 hMSCs with (D) approximately 2000 cubes and (E) approximately 700 donuts shows minimal cell death after 14 days of culture. SEM images show a compact assembly of (F, G) cubes or (H) donuts with hMSCs after 1 week of culture. (F) One aggregate was disrupted on purpose to be able to study the core of the aggregate. It can be seen that the core of the aggregate shows a certain degree of porosity with cells homogeneously distributed between the objects while the outside of the aggregate is fully covered with a dense cell sheet. (H) In some aggregates, micro-objects were found on the outer layer of the aggregate. Yet, in most aggregates, all objects are fully integrated under a dense layer of cells and ECM. (I–J) These results are confirmed by histological analysis where a homogeneous distribution of cells and objects is found in the core of the aggregate, while the exterior shows multiple layers of cellular and extracellular matter. The box in (I) indicates the area displayed at higher magnification in (J). The aggregates in (D) and (E) show a diameter of approximately 600 μm. The scale bars represent (A–C, F, J) 100 μm, (G) 20 μm, (H) 50 μm, and (I) 500 μm. hMSCs, human bone marrow stromal cells; SEM, scanning electron microscopy; ECM, extracellular matrix.

3.3. Cell viability during culture with micro-objects

The absence of photochemistry-based toxic traces increases the possibilities for clinical translation of the objects in multiple applications in the field of TE and regenerative medicine. To investigate cytotoxicity, approximately 2000 cube- and 700 donut-shaped objects were combined with 5×10^4 hMSCs on a cell-repellent agarose layer, which was added to conventional 96-well plates. The number of micro-objects was corrected for the volume of each type of micro-object to make sure that the total volume of objects per well is kept constant in each well. Figs. 3D (cubes) and E (donuts) show fluorescent microscopy images with the focal plane at the widest part of the aggregate, which should correspond to approximately the half height of the aggregate. Because it is not a confocal image, the signal observed is retrieved from the aggregate as a whole. The aggregates with a diameter of around 600 μm after 14 days of culture show viable cells in green and dead cells in red. Although the donuts theoretically introduce more pore volume in a tissue construct than the cubes, which may optionally lead to a higher cell viability, no differences in viability as a result of this pore volume were observed. It can be observed that the majority of cells combined with micro-objects are viable. Higher magnification images and split channels (green = live, red = dead) confirm this finding for 3, 7, and 14 days of culture (Figs. S4, S5, and S6, respectively). Furthermore, the results of controls in the form of aggregates from only 5×10^4 cells and from 5×10^4 cells combined with approximately 2800 PDLLA microspheres, fabricated by an emulsion-solvent-based extraction method (supplementary information) without oxygen plasma treatment of the spheres, show similar degrees of viability (Figs. S4–6). Yet, the aggregates formed from cells only without the presence of micro-objects or microspheres show smaller diameters after 7 and 14 days of culture, indicating that the addition of objects and spheres indeed allows for larger-sized tissue constructs without the requirement of adding more cells.

Other studies on cells-only aggregates show aggregate diameters up to approximately 600 μm while maintaining viabilility [43,44]. Rivron et al. [27] introduced an approach to prevascularize microtissues through cell assembly in agarose microwells to potentially overcome cell death related to nutrient deficiency. Yet, their method required multiple sequential assembly steps. Although the resulting tissue constructs showed early indications of vascularization, no evidence for an interconnected vascular network was found. Recently, Vrij et al. [26] have shown to challenge the critical size of *in vitro* cultured tissue constructs via a cell-only bottom-up approach. In both studies by Rivron et al. [27] and Vrij et al. [26], the assemblies were exceeding diffusion limits in the lateral direction only, while the thickness of the constructs remained beyond a critical size where nutrient supply to the inner cells by diffusion was still possible. Furthermore, in the mentioned studies and in other studies on scaffold-free bottom-up TE, high numbers of cells were required to be able to form tissues with clinically relevant volumes [28, 45]. On the contrary, in the method presented here, submillimeter-sized tissue constructs can already be obtained in a one- or two-step procedure within 3–4 days of culture with a relatively low cell number. Supported by the cell-assembled micro-objects scaffold, the resulting aggregates show sufficient mechanical stability to be transferred by means of pipetting or tweezers.

3.4. Cell-guided assembly of the micro-objects

In Figs. 3F–H, scanning electron microscopy (SEM) images show the high degree of integration of the cells and the micro-objects. From the inner part of the aggregate (Fig. 3F and Fig. S7), it can be observed that the cells are homogeneously distributed between the micro-objects throughout the aggregate. Only on the outside of the aggregate, a dense skin layer of (only) cells and ECM is observed, which is confirmed by histological analysis (Fig. 3I). This dense layer corresponds to results found in other studies on the self-assembly of cells in cell-only bottom-up TE approaches and is suspected to be related to geometry-induced

processes in the actin-myosin complex [27]. In some aggregates, this layer reached thicknesses of more than 30 μm (Figs. 3I and J). Although this relatively thick and dense layer may reduce the tissue diffusivity, histological analysis shows no evidence for cell death in the form of a necrotic core in aggregates that reach up to millimeter-sized diameters.

As indicated, permeability of the obtained tissue constructs is of paramount importance in sustaining viable and functional cells within the constructs. The circularity of the aggregates can be determined as an indirect measure for tissue compaction and therewith tissue diffusivity assuming a homogeneous tissue density throughout the aggregate. Furthermore, changes in circularity over time and fusion of aggregates after compaction are indications of active tissue remodeling, which is essential, for example, in the musculoskeletal area. Fig. 4A addresses the circularity of aggregates in various conditions with cube-shaped micro-objects after image analysis of a series of 2D phase-contrast images (Figs. S8–11). It can be observed that aggregates' circularity depends on the cell type used, the ratio of cells to objects, and the culture method – coculture by mixing or by a 2-day later addition of a second cell type (referred to as 'mixed' and 'added', respectively, see next paragraph). Furthermore, it was observed that the circularity of the formed aggregates increased over time for almost all conditions. These results correspond to previous results on SU-8–based micro-objects in which the circularity of the aggregates showed to be dependent on the ratio of cells to objects, the object size and shape, and the cell type used [14].

3.5. Coculture of hMSCs and endothelial cells on micro-objects

Previously, it has been shown that mechanical forces, among others compressive forces, can result in apoptosis in various cell types [46–48]. Here, cell death induced as a result of such forces during cellular assembly is expected to be limited because of the objects' geometry-based compaction hindrance. Yet, cell death resulting from diffusion limitations in large-sized tissue constructs when cultured for multiple days may occur. Therefore, vascularization remains a process of vital importance in upscaling to the millimeter or even centimeter range [49]. McGuigan and Sefton [49] have reported the application of an endothelial cell layer around hepatocytes-laden gelatin-based modular tissue constructs. By exposing the endothelial cells to the desired shear stress, they aimed at obtaining a non-thrombogenic phenotype of the cells. Unfortunately, the authors were confronted with low cell viabilities probably because of the cross-linking method introduced to obtain the gelatin gels. Nevertheless, approaches to obtain sufficient blood perfusability in tissue-engineered constructs by introducing endothelial cells have shown promising results [50]. Here, to explore the possibilities of introducing vascular endothelial cells as a first approach toward vascularization, HUVECs were applied in combination with hMSCs and micro-objects.

The order of adding the two cell types to the micro-objects determined the rate and compaction of the cell-guided assembly, the resulting cellular organization, and the cell survival (Fig. 4A). When 2.5×10^4 HUVECs were added to 10,000, 5000, or 2500 cube-shaped micro-objects, hardly any cell attachment, assembly, and compaction was observed (Fig. S9). In Figs. S12–14, it can be observed that when HUVECs (stained green) and hMSCs (stained red) were mixed in a 1:1 ratio, within 3 days of culture, the number of HUVECs significantly drops compared with the number of hMSCs. This effect is independent of the ratio of cells to objects. From these data, it becomes clear that hMSCs are the driving force in tissue compaction and remodeling. When a coculture of hMSCs and HUVECs shall be established, the order of adding cells to the objects and the cell numbers will have to be optimized.

When 3×10^4 HUVECs were added to an approximately 1-mm-large 1-day–cultured preaggregated tissue construct of 3×10^4 hMSCs and approximately 3000 cube-shaped micro-objects, they showed to adhere to the construct and form a coating around the aggregate (Fig. 4B). This cell layer of HUVECs disintegrated a few days later, and the detached HUVECs seem to undergo cell death. Yet, when multiple smaller 4-
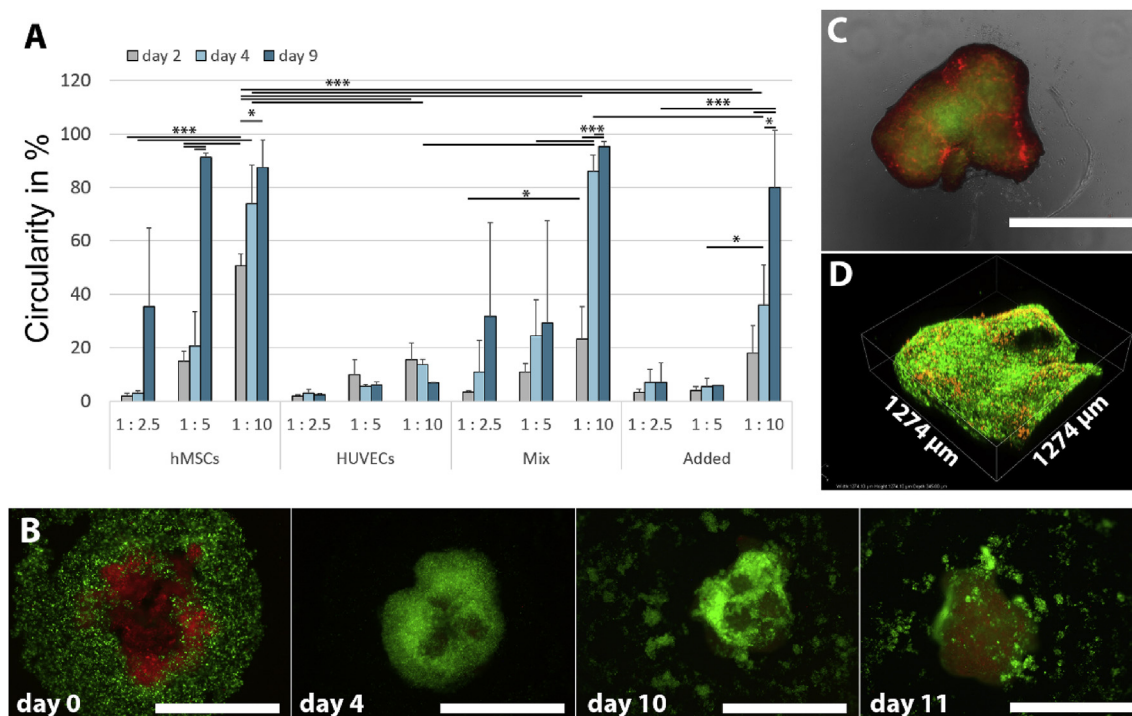
Fig. 4. (A) Circularity quantified by image analysis of aggregates formed at various object-to-cell ratios of 1:2.5, 1:5, and 1:10 obtained by introducing 10,000, 5000, and 2500 cube-shaped objects per well, respectively (n = 3). ('hMSCs') For aggregates of only 2.5×10^4 hMSCs and micro-objects, a significant increase in circularity is found over time and with lower object-to-cell ratios. ('HUVECs') For aggregates of 2.5×10^4 HUVECs and objects, a lower object-to-cell ratio increases the circularity as well. Yet, the circularity of the formed aggregate is significantly lower than for hMSCs and does not increase over time. ('Mix') When the two cell types are mixed in a 1:1 ratio before addition to the micro-objects, after 9 days, the circularity reaches similar levels as for hMSCs only, indicating that the hMSCs are able to compensate for the limited aggregation behavior of the HUVECs. ('Added') However, when 1.25×10^4 HUVECs are added to a preaggregate of 1.25×10^4 hMSCs and micro-objects that was cultured for 1 day, the subsequent aggregation behavior seems to be compromised, even when one would normalize to the absolute number of seeded hMSCs. (B) 3×10^4 hMSCs were stained red and allowed to preaggregate with approximately 3000 cube-shaped micro-objects for 1 day before adding 3×10^4 green-stained HUVECs (final object-to-cell ratio: 1:20). It can be observed that the HUVECs form a layer around the hMSCs within 4 days of culture. Yet, this layer disintegrates after day 10, and the HUVECs show a decrease in viability and number. (C) Four green-stained 4-day-old aggregates of 1×10^4 hMSCs and approximately 500 donut-shaped micro-objects were complemented with 2.5×10^3 red-stained HUVECs per aggregate and transferred to a hemispherically shaped cell-repellent agarose layer one day later and cultured for another 7 days. It can be observed that the HUVECs stay aligned in between the preaggregates. (D) Confocal fluorescence image of the surface of the aggregate shown in (C). The scale bars represent 1 mm. The height of the scanned area in (D) is 345 μm. * indicates a p-value < 0.05, ** indicates a p-value < 0.01, and *** indicates a p-value < 0.001. hMSCs, human bone marrow stromal cells; HUVECs, human umbilical vein endothelial cells.

day–cultured precompacted aggregates from 1×10^4 hMSCs and approximately 500 donut-shaped objects were combined each with 2.5×10^3 HUVECs and were allowed to assemble after 1 day, the HUVECs did not disintegrate but stay aligned as HUVEC-rich regions at the aggregates' interfaces (Figs. 4C and D and Figs. S15 and S16). This 3D network-type spatial cellular organization could foster the establishment of (premature) vascular structures as a vital prerequisite of, for example, bottom-up-engineered bone-like tissue. Our approach is supported by studies on vascularization in conjunction with bottom-up TE by Zhong et al. [9] and McGuigan et al. [50]. Yet, those studies are still based on classical hydrogel building blocks in which the non-endothelial cells are fully embedded in the gel.

To further control the spatial organization of multiple cell types during cell-guided assembly, a cell-repellent microwell array from agarose gel was fabricated to therein combine micro-objects, hMSCs, and HUVECs (Fig. S17). Still based on conventional cells-only aggregation, Tekin et al. [51] showed a partially similar approach, yet their system is more complicated because it requires microwells having temperature-dependent dynamic properties. Here, we show that a static microwell system is a promising tool in obtaining spatial control in cellular assemblies upon sequential seeding of two cell types. It can be observed that HUVECs form a layer around the micro-aggregates of hMSCs and micro-objects. Optimization of cell numbers, culture conditions, and methods of fusing multiple micro-aggregates may aid in the formation of prevascularized complex tissue assemblies.

3.6. Surface functionalization of the micro-objects for bone TE

As a proof of concept for the functionalization of PDLLA micro-objects for bone TE, we coated the objects with octacalciumphosphate (OCP) (Fig. S18). OCP is known as an osteoconductive material allowing for the integration of surrounding bone with the implanted or injected substitute material. Other methods of functionalization of the micro-objects' surfaces can involve, for example, instructive nanotopographies, chemical modifications by plasma treatments or in the form of peptide-functionalized coatings, or drug delivery coatings. Furthermore, the cell and micro-object assemblies can potentially be complemented with hydrogels as another functional (e.g. binding, viscosity-determining or drug-loaded) phase [52]. In the future, by combining the micro-objects with other instructive or smart materials, novel advanced TE approaches and a broad range of potential applications can be explored.

4. Conclusions

In summary, we present a bottom-up TE approach utilizing engineered micro-objects with tailorable shapes and sizes on which cells can adhere and that can aid in the formation of viable tissue constructs of clinically relevant size. The micro-objects were successfully created by a novel, photoinitiator-free, thermal imprinting-based process conducted on a water-soluble sacrificial layer for the later release of the objects, onto which before the material for the creation of the objects has been

transferred in the form of a film. The process allows the material to be chosen from a wide variety of thermoplastic biomaterials, such as exemplarily PDLLA in case of this study, depending on the demands imposed by the specific research question or clinical application. The latter may range from advanced bone fillers to cell expansion carriers, and beyond. Here, we show the applicability of the objects in *in vitro* culture settings, including hMSCs and HUVECs as representative cell sources in TE, and as spacer material to reduce the required number of patient-derived cells in potential future cell-based TE therapies.

Conflict of interest

The authors declare that they have no known competing financial interests or personal relationships that could have appeared to influence the work reported in this paper.

Acknowledgements

Appendix A. Supplementary data

Supplementary data to this article can be found online at https://doi.org/10.1016/j.mtbio.2019.100025.

References

[1] R. Langer, J.P. Vacanti, Tissue engineering, Science 260 (5110) (1993) 920–926, https://doi.org/10.1126/science.8493529.
[2] V. Marx, Tissue engineering: organs from the lab, Nature 522 (7556) (2015) 373–377, https://doi.org/10.1038/522373a.
[3] L. Moroni, et al., Chapter 1 – Tissue engineering: an introduction, in: C. van Blitterswijk (Ed.), Tissue Engineering, Academic Press, 2014, pp. 1–21.
[4] J.W. Nichol, A. Khademhosseini, Modular tissue engineering: engineering biological tissues from the bottom up, Soft Matter 5 (7) (2009) 1312–1319, https://doi.org/10.1039/b814285h.
[5] D.L. Elbert, Bottom-up tissue engineering, Curr. Opin. Biotechnol. 22 (5) (2011) 674–680, https://doi.org/10.1016/j.copbio.2011.04.001.
[6] S. Guven, et al., Multiscale assembly for tissue engineering and regenerative medicine, Trends Biotechnol. 33 (5) (2015) 269–279, https://doi.org/10.1016/j.tibtech.2015.02.003.
[7] A.M. Leferink, et al., Distribution and viability of fetal and adult human bone marrow stromal cells in a biaxial rotating vessel bioreactor after seeding on polymeric 3D additive manufactured scaffolds, Front Bioeng. Biotechnol. 3 (2015) 169, https://doi.org/10.3389/fbioe.2015.00169.
[8] A.P. McGuigan, et al., Cell encapsulation in sub-mm sized gel modules using replica molding, PLoS One 3 (5) (2008) e2258, https://doi.org/10.1371/journal.pone.0002258.
[9] M. Zhong, et al., Vascularization in engineered tissue construct by assembly of cellular patterned micromodules and degradable microspheres, ACS Appl. Mater. Interfaces 9 (4) (2017) 3524–3534, https://doi.org/10.1021/acsami.6b15697.
[10] J. Groll, et al., Biofabrication: reappraising the definition of an evolving field, Biofabrication 8 (1) (2016) 013001, https://doi.org/10.1088/1758-5090/8/1/013001.
[11] A. Khademhosseini, R. Langer, Microengineered hydrogels for tissue engineering, Biomaterials 28 (34) (2007) 5087–5092, https://doi.org/10.1016/j.biomaterials.2007.07.021.
[12] J.A. Hunt, et al., Hydrogels for tissue engineering and regenerative medicine, J. Mater. Chem. B 2 (33) (2014) 5319–5338, https://doi.org/10.1039/c4tb00775a.
[13] D.R. Griffin, et al., Accelerated wound healing by injectable microporous gel scaffolds assembled from annealed building blocks, Nat. Mater. 14 (7) (2015) 737–744, https://doi.org/10.1038/nmat4294.
[14] A. Leferink, et al., Engineered micro-objects as scaffolding elements in cellular building blocks for bottom-up tissue engineering approaches, Adv. Mater. 26 (16) (2014) 2592–2599, https://doi.org/10.1002/adma.201304539.
[15] M. Hennemeyer, et al., Cell proliferation assays on plasma activated SU-8, Microelectron. Eng. 85 (5–6) (2008) 1298–1301, https://doi.org/10.1016/j.mee.2008.01.026.
[16] C. Hassler, T. Boretius, T. Stieglitz, Polymers for neural implants, J. Polym. Sci. B Polym. Phys. 49 (1) (2011) 18–33, https://doi.org/10.1002/polb.22169.

[17] Q. Wang, et al., Hybrid hydroxyapatite nanoparticle colloidal gels are injectable fillers for bone tissue engineering, Tissue Eng. Part A 19 (23–24) (2013) 2586–2593, https://doi.org/10.1089/ten.TEA.2013.0075.
[18] L.F. Peng, et al., Micro hot embossing of thermoplastic polymers: a review, J. Micromech. Microeng. 24 (1) (2014), https://doi.org/10.1088/0960-1317/24/1/013001.
[19] L.J. Guo, Nanoimprint lithography: methods and material requirements, Adv. Mater. 19 (4) (2007) 495–513, https://doi.org/10.1002/adma.200600882.
[20] S.Y. Chou, P.R. Krauss, P.J. Renstrom, Imprint lithography with 25-nanometer resolution, Science 272 (5258) (1996) 85–87, https://doi.org/10.1126/science.272.5258.85.
[21] S. Hasegawa, et al., In vivo evaluation of a porous hydroxyapatite/poly-DL-lactide composite for bone tissue engineering, J. Biomed. Mater. Res. A 81 (4) (2007) 930–938, https://doi.org/10.1002/jbm.a.31109.
[22] C. Gayer, et al., Development of a solvent-free polylactide/calcium carbonate composite for selective laser sintering of bone tissue engineering scaffolds, Mater. Sci. Eng. C Mater. Biol. Appl. 101 (2019) 660–673, https://doi.org/10.1016/j.msec.2019.03.101.
[23] H.V. Unadkat, et al., An algorithm-based topographical biomaterials library to instruct cell fate, Proc. Natl. Acad. Sci. U.S.A. 108 (40) (2012), https://doi.org/10.1073/pnas.1109861108, 5905-5905.
[24] M.J. Dalby, et al., The control of human mesenchymal cell differentiation using nanoscale symmetry and disorder, Nat. Mater. 6 (12) (2007) 997–1003, https://doi.org/10.1038/nmat2013.
[25] R. McBeath, et al., Cell shape, cytoskeletal tension, and RhoA regulate stem cell lineage commitment, Dev. Cell 6 (4) (2004) 483–495, https://doi.org/10.1016/S1534-5807(04)00075-9.
[26] E. Vrij, et al., Directed assembly and development of material-free tissues with complex architectures, Adv. Mater. 28 (21) (2016) 4032–4039, https://doi.org/10.1002/adma.201505723.
[27] N.C. Rivron, et al., Tissue deformation spatially modulates VEGF signaling and angiogenesis, Proc. Natl. Acad. Sci. U. S. A. 109 (18) (2012) 6886–6891, https://doi.org/10.1073/pnas.1201626109.
[28] A.D. Dikina, et al., A modular strategy to engineer complex tissues and organs, Adv. Sci. 5 (5) (2018) 1700402, https://doi.org/10.1002/advs.201700402.
[29] J.D. de Bruijn, et al., Bone induction by implants coated with cultured osteogenic bone marrow cells, Adv. Dent. Res. 13 (1999) 74–81, https://doi.org/10.1177/08959374990130011801.
[30] J. Schindelin, et al., Fiji: an open-source platform for biological-image analysis, Nat. Methods 9 (7) (2012) 676–682, https://doi.org/10.1038/Nmeth.2019.
[31] H. Yoon, H. Lee, W.B. Lee, Toward residual-layer-free nanoimprint lithography in large-area fabrication, Korea-Aust. Rheol. J. 26 (1) (2014) 39–48, https://doi.org/10.1007/s13367-014-0005-5.
[32] F.C.N. Hong, Y.C. Kao, Residual-layer-free printing by selective filling of self-assembled monolayer-treated mold, J. Vac. Sci. Technol. B 29 (4) (2011), https://doi.org/10.1116/1.3596558.
[33] W. Jiang, H. Liu, Y. Ding, Selective-filling mold for residual-layer-free patterning of 3D microstructures, Mater. Manuf. Process. 28 (1) (2012) 101–105, https://doi.org/10.1080/10426914.2012.709342.
[34] Y.-C. Kao, F.C.-N. Hong, Residual-layer-free direct printing by selective filling of a mould, J. Micromech. Microeng. 21 (2) (2011) 025026, https://doi.org/10.1088/0960-1317/21/2/025026.
[35] R. Kuduva-Raman-Thanumoorthy, D.G. Yao, Hot embossing of discrete microparts, Polym. Eng. Sci. 49 (10) (2009) 1894–1901, https://doi.org/10.1002/pen.21422.
[36] R.S. Petersen, et al., Hot embossing and mechanical punching of biodegradable microcontainers for oral drug delivery, Microelectron. Eng. 133 (2015) 104–109, https://doi.org/10.1016/j.mee.2014.11.009.
[37] L. Moroni, L.P. Lee, Micropatterned hot-embossed polymeric surfaces influence cell proliferation and alignment, J. Biomed. Mater. Res. A 88 (3) (2009) 644–653, https://doi.org/10.1002/jbm.a.31915.
[38] Y. Zhao, et al., High-definition micropatterning method for hard, stiff and brittle polymers, Mater. Sci. Eng. C Mater. Biol. Appl. 71 (2017) 558–564, https://doi.org/10.1016/j.msec.2016.11.004.
[39] R. Truckenmuller, et al., Fabrication of cell container arrays with overlaid surface topographies, Biomed. Microdevices 14 (1) (2012) 95–107, https://doi.org/10.1007/s10544-011-9588-5.
[40] K.S. Brammer, et al., Hydrophobic nanopillars initiate mesenchymal stem cell aggregation and osteo-differentiation, Acta Biomater. 7 (2) (2011) 683–690, https://doi.org/10.1016/j.actbio.2010.09.022.
[41] M. Nikkhah, et al., Cytoskeletal role in differential adhesion patterns of normal fibroblasts and breast cancer cells inside silicon microenvironments, Biomed. Microdevices 11 (3) (2009) 585–595, https://doi.org/10.1007/s10544-008-9268-2.
[42] A.K. Nguyen, R.J. Narayan, Two-photon polymerization for biological applications, Mater. Today 20 (6) (2017) 314–322, https://doi.org/10.1016/j.mattod.2017.06.004.
[43] A.C. Tsai, et al., Compaction, fusion, and functional activation of three-dimensional human mesenchymal stem cell aggregate, Tissue Eng. Part A 21 (9–10) (2015) 1705–1719, https://doi.org/10.1089/ten.TEA.2014.0314.
[44] W.L. Zhang, et al., Optimization of the formation of embedded multicellular spheroids of MCF-7 cells: how to reliably produce a biomimetic 3D model, Anal. Biochem. 515 (2016) 47–54, https://doi.org/10.1016/j.ab.2016.10.004.
[45] C.M. Livoti, J.R. Morgan, Self-assembly and tissue fusion of toroid-shaped minimal building units, Tissue Eng. Part A 16 (6) (2010) 2051–2061, https://doi.org/10.1089/ten.TEA.2009.0607.

[46] R. Gupta, O. Steward, Chronic nerve compression induces concurrent apoptosis and proliferation of Schwann cells, J. Comp. Neurol. 461 (2) (2003) 174–186, https://doi.org/10.1002/cne.10692.

[47] M.H. Hsieh, H.T. Nguyen, Molecular mechanism of apoptosis induced by mechanical forces, Int. Rev. Cytol. 245 (2005) 45–90, https://doi.org/10.1016/S0074-7696(05)45003-2.

[48] K. Ariga, et al., Mechanical stress-induced apoptosis of endplate chondrocytes in organ-cultured mouse intervertebral discs: an ex vivo study, Spine 28 (14) (2003) 1528–1533, https://doi.org/10.1097/01.BRS.0000076915.55939.E3.

[49] A.P. McGuigan, M.V. Sefton, Vascularized organoid engineered by modular assembly enables blood perfusion, Proc. Natl. Acad. Sci. U.S.A. 103 (31) (2006) 11461–11466, https://doi.org/10.1073/pnas.0602740103.

[50] A.P. McGuigan, M.V. Sefton, Modular tissue engineering: fabrication of a gelatin-based construct, J. Tissue Eng. Regen. Med. 1 (2) (2007) 136–145, https://doi.org/10.1002/term.14.

[51] H. Tekin, et al., Controlling spatial organization of multiple cell types in defined 3D geometries, Adv. Mater. 24 (41) (2012) 5543–5547, https://doi.org/10.1002/adma.201201805.

[52] F. Song, et al., Nanocomposite hydrogels and their applications in drug delivery and tissue engineering, J. Biomed. Nanotechnol. 11 (1) (2015) 40–52, https://doi.org/10.1166/jbn.2015.1962.